Study of the radiative decay $K^+ \to \mu^+ \nu\gamma$

Y. Akiba, T. Ishikawa, M. Iwasaki, K. H. Tanaka, S. Ohtake, H. Tamura,
M. Nakajima, T. Yamanaka, and T. Yamazaki
Department of Physics and Meson Science Laboratory, University of Tokyo, Bunkyo-ku, Tokyo 113, Japan

F. Naito and T. Suzuki
Department of Applied Physics, Tokyo Institute of Technology, Ookayama, Meguro-ku, Tokyo 152, Japan

I. Arai
Institute of Physics, University of Tsukuba, Sakura-mura, Niihari-gun, Ibaraki 305, Japan

R. S. Hayano
National Laboratory for High Energy Physics, Oho-machi, Tsukuba-gun, Ibaraki 305, Japan
(Received 7 June 1985)

The radiative decay $K^+ \to \mu^+ \nu\gamma$ has been studied by a high-resolution magnetic spectrometer combined with a NaI(Tl) photon detector system. The momentum spectrum of muon from this decay mode was measured in the region $214.5 < p_\mu < 231.5$ MeV/c. The observed partial decay rate of the radiative decay in this region agreed with the QED calculation within the error of 3%. The structure-dependent components of the decay were studied and new values of the form factors were obtained as $|F_V + F_A|_{(\mu)} M_K < 0.23$, $-2.5 < (F_V - F_A)_{(\mu)} M_K < 0.3$. By using these bounds the branching ratio was determined as $B(K_{\mu\nu\gamma}, p_\mu < 231.5 \text{ MeV}/c) = (5.4 \pm 0.3) \times 10^{-3}$.

I. INTRODUCTION

The radiative decay $K^+ \to l^+ \nu\gamma (l = e, \mu)$ provides interesting information on the properties of hadronic weak currents. Since the final state of the decay consists of leptons and photons we can probe the properties of a hadronic weak current in the low-energy region without final-state strong interactions.

The following terms contribute to this decay mode; the internal-bremsstrahlung (IB) term, the structure-dependent (SD) term, and the interference (INT) term between them. The structure-dependent amplitude can be written[1] in terms of the vector form factor (F_V) and the axial-vector form factor (F_A). We can determine the magnitude and the phase of both form factors simultaneously by studying this decay process and there are many theoretical works on these form factors.[1]

However, only a few experiments have been done. For the $K_{e\nu\gamma}$ mode, two experiments were performed at the CERN proton synchrotron (PS) and the values of the form factors were obtained to be[2]

$$|F_V + F_A|_{(e)} M_K = 0.153 \pm 0.011 , \tag{1a}$$

$$|F_V - F_A|_{(e)} M_K < 0.5 . \tag{1b}$$

Though this experiment gave a strong constraint on the magnitude of $F_V + F_A$, the uncertainty on $F_V - F_A$ was large and so one could not independently determine the values of the vector and axial-vector form factors.

For the $K_{\mu\nu\gamma}$ mode, there was only one direct measurement[3] which determined a branching ratio as

$$B(K_{\mu\nu\gamma}, E_\gamma > 9 \text{ MeV}) = (5.8 \pm 3.5) \times 10^{-3} . \tag{2}$$

This value could be explained in terms of the IB component only and gave almost no constraint on the form factors.

In the present work, we have measured the $K_{\mu\nu\gamma}$ mode much more precisely. The purpose of this study is (i) to present the first high-statistics counter experiment on this decay mode and to compare the measurement to the theory, and (ii) to search for the effects of structure-dependent amplitude in the decay spectrum. For the second purpose we searched for the effects of the interference term as well as the structure-dependent term. It should be noted that the measurement of the INT term is very important for the determination of the form factors because one can determine the sign of the decay amplitude as well as its magnitude. However, in the case of the $K_{e\nu\gamma}$ decay mode, it is practically impossible to determine the sign of the form factors because the INT term is negligibly small. The possibility of measuring the INT term is a unique feature of the $K_{\mu\nu\gamma}$ mode.

The experiment was performed as a byproduct of a series of experiments[4] to search for heavy neutrinos and other exotic particles in the decay of K^+. The experimental setup permitted high-resolution spectroscopy of muon momentum together with very efficient photon detection; thus it was very suitable for the present purpose.

In the next section, the theory and the kinematics are described as a basis of the present study. In Sec. III, the apparatus of the experiment is described. In Sec. IV, we describe the procedure of the analysis and the experimental results will be presented.

II. THEORY AND KINEMATICS

In this section we describe briefly the kinematics of the decay and explain the principle of the experiment. In the framework of the standard theory, the decay rate of the $K_{\mu\nu\gamma}$ in the K^+ rest frame is written as[1]

$$\frac{d^2W}{dx\,dy} = A_{\rm IB} f_{\rm IB}(x,y) + A_{\rm SD}[(F_V+F_A)^2 f_{\rm SD_+}(x,y) + (F_V-F_A)^2 f_{\rm SD_-}(x,y)]$$
$$+ A_{\rm INT}[(F_V+F_A) f_{\rm INT_+}(x,y) + (F_V-F_A) f_{\rm INT_-}(x,y)] , \tag{3}$$

where

$$f_{\rm IB}(x,y) = \left[\frac{1-y+r}{x^2(x+y-1-r)}\right] \times \left[x^2+2(1-x)(1-r)-\frac{2xr(1-r)}{x+y-1-r}\right] , \tag{4a}$$

$$f_{\rm SD_+}(x,y) = [x+y-1-r][(x+y-1)(1-x)-r] , \tag{4b}$$

$$f_{\rm SD_-}(x,y) = [1-y+r][(1-x)(1-y)+r] , \tag{4c}$$

$$f_{\rm INT_+}(x,y) = \left[\frac{1-y+r}{x(x+y-1-r)}\right][(1-x)(1-x-y)+r] , \tag{4d}$$

$$f_{\rm INT_-}(x,y) = \left[\frac{1-y+r}{x(x+y-1-r)}\right] \times [x^2-(1-x)(1-x-y)-r] , \tag{4e}$$

$$x = \frac{2E_\gamma}{M_K} , \tag{4f}$$

$$y = \frac{2E_\mu}{M_K} , \tag{4g}$$

$$r = \left[\frac{m_\mu}{M_K}\right]^2 , \tag{4h}$$

$$A_{\rm IB} = W_{K\mu 2}\frac{\alpha}{2\pi}\frac{1}{(1-r)^2} , \tag{4i}$$

$$A_{\rm SD} = W_{K\mu 2}\frac{\alpha}{8\pi}\frac{1}{r(1-r)^2}\left[\frac{M_K{}^2}{F_K}\right]^2 , \tag{4j}$$

$$A_{\rm INT} = W_{K\mu 2}\frac{\alpha}{2\pi}\frac{1}{(1-r)^2}\frac{M_K}{F_K} . \tag{4k}$$

In these formulas, F_V is the vector form factor and F_A is the axial-vector form factor, α is the fine-structure constant ($=1/137.036$), $W_{K\mu 2}$ is the decay rate of the $K^+\to\mu^+\nu$ mode, and F_K is the decay constant of K^+ ($=161$ MeV). In this formulation, we have assumed T invariance which requires that both form factors are real. We have also neglected the q^2 dependence of the form factors. In formula (3), the terms proportional to $A_{\rm IB}$, $A_{\rm SD}$, $A_{\rm INT}$ correspond to the following three components contributing to the $K_{\mu\nu\gamma}$ decay.

(a) Internal bremsstrahlung (IB). This is a radiative correction to the $K_{\mu 2}$ decay and the decay rate of this component can be calculated by quantum electrodynamics. Feynman diagrams contributing to IB component are illustrated in Fig. 1. This component dominates in most parts of the kinematical region of the $K_{\mu\nu\gamma}$ decay because the $K_{\mu 2}$ decay is the dominant decay branch of K^+ (branching ratio $=63.5\%$).

(b) Structure-dependent (SD) term. The photon is emitted from intermediate states governed by strong interactions. As shown in the formula (3), the SD component is separated into two terms which are proportional to $(F_V+F_A)^2$ and $(F_V-F_A)^2$. We call them the $\rm SD_+$ and $\rm SD_-$ terms. The $\rm SD_+$ and $\rm SD_-$ terms correspond to the emission of photons with positive and negative helicities, respectively.

(c) Interference (INT) term. This is the result of the interference between the IB amplitude and the SD amplitude. The interference component is also separated into two parts which are proportional to F_V+F_A ($\rm INT_+$ term) and F_V-F_A ($\rm INT_-$ term).

These five terms have very different Dalitz plots, as shown in Figs. 2(a)–2(e). For example, the Dalitz plot of the IB term has a very large population around the kinematical boundary of the low-energy photon emission [Fig. 2(a)], while that of the $\rm SD_+$ term has a broad peak around $E_\gamma=170$ MeV and $p_\mu=235.5$ MeV/c [Fig. 2(b)].

Therefore, in principle, we can determine the strength of each term by choosing a suitable kinematical region of observation. However, experimentally, the situation is not

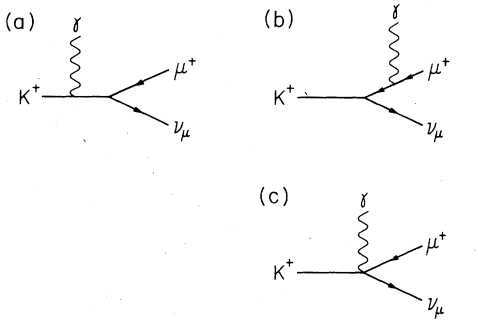

FIG. 1. Feynman diagrams contributing to the IB term. (c) shows a contact term which appears because K^+ is a boson. This graph ensures the gauge invariance of the decay amplitude.

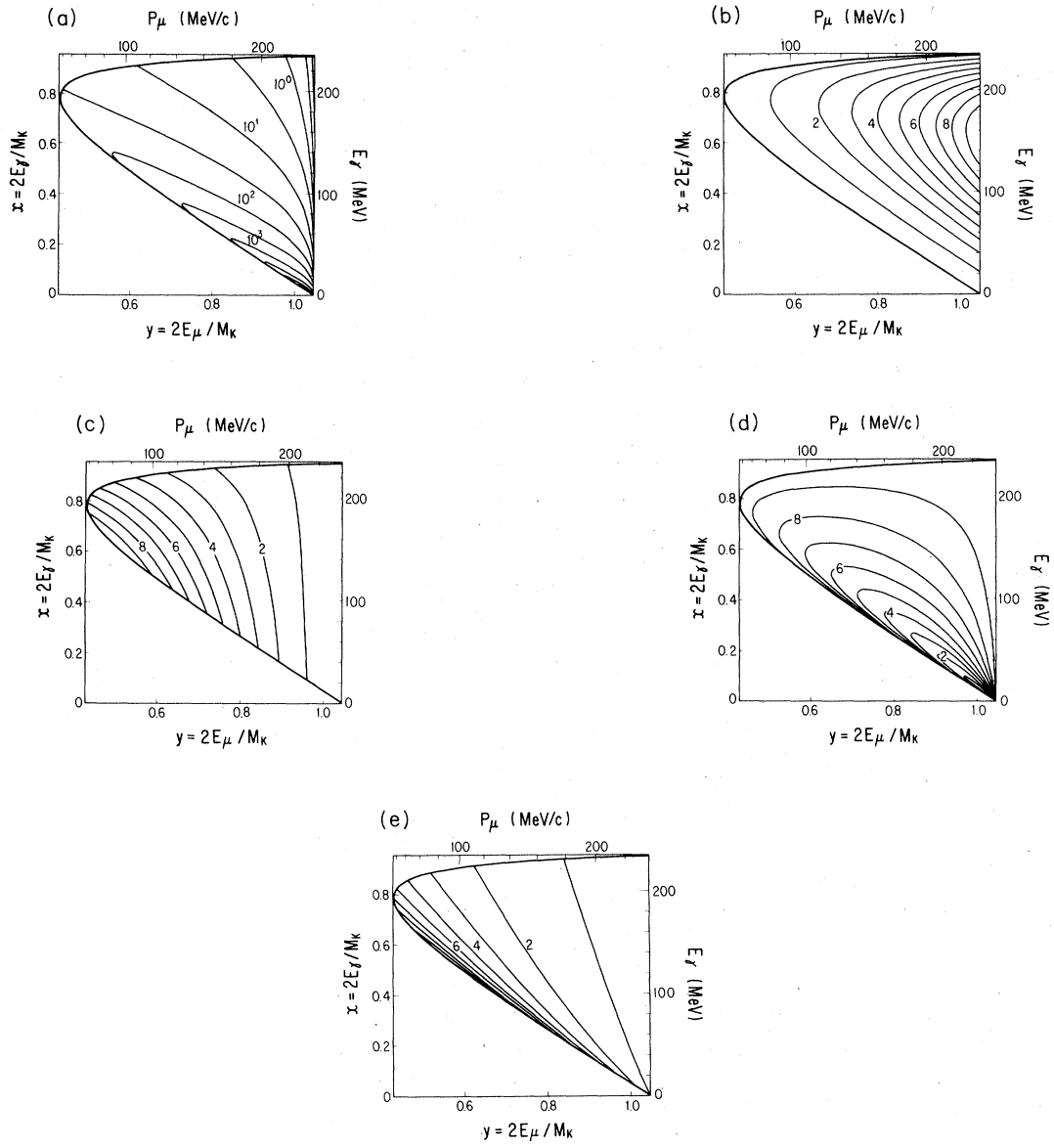

FIG. 2. Dalitz plots for the (a) IB term, (b) SD_+ term, (c) SD_- term, (d) INT_+ term, and (e) INT_- term. The units are arbitrary.

so simple. The kinematical region feasible for the study is restricted by the background from the $K_{\mu 3}$ decay ($p_\mu < 215$ MeV/c) and the K_{e3} decay ($p_e < 228$ MeV/c).

Considering the characteristics of each term and the restrictions from the background, we chose the kinematical region for the observation of each component as described below.

(i) Study of the IB component. We chose the kinematical region

$$214.5 \text{ MeV}/c < p_\mu < 231.5 \text{ MeV}/c \ , \tag{5}$$

to measure the IB term. This region is free from the background of the $K_{\mu 3}$ decay, and thus is very suitable for the measurement. The high-momentum resolution [1.6 MeV/c full width at half maximum (FWHM)] and the large photon detection efficiency (85% for photons from the $K_{\mu\nu\gamma}$ mode) of our apparatus allowed us to identify the $K_{\mu\nu\gamma}$ event unambiguously.

(ii) Search for the SD_+ contribution. We chose the region

$$216 < p_\mu < 230 \text{ MeV}/c \ , \tag{6a}$$

$$100 \text{ MeV} < E_\gamma \ , \tag{6b}$$

to search for the effect of SD_+ term.

When we integrate over the momentum region (6a) the differential decay rate for each term relative to the $K_{\mu 2}$ total decay rate is determined as a function of the photon

energy (E_γ) as shown in Fig. 3(a). The differential decay rate of the SD_+ term has a broad peak around $E_\gamma = 170$ MeV, while that of the IB term decreases very rapidly with the increase of the photon energy. Moreover, the contributions from other terms are small. Thus, this region is most sensitive to the SD_+ term.

(iii) Study of INT_ and SD_ terms

We searched for the effect of the INT_ and the SD_ terms in the kinematical region

$$120 < p_\mu < 150 \text{ MeV}/c \ . \tag{7}$$

As shown in Fig. 3(b), these two terms have maxima around $p_\mu = 120$ MeV/c, while the strength of the IB term decreases as p_μ decreases. Therefore, the region with low p_μ is suitable for the detection of these two terms. However, there is a serious background from the $K_{\mu 3}$ decay which is much more frequent than the $K_{\mu\nu\gamma}$ decay.

In order to discriminate the $K_{\mu\nu\gamma}$ signal from the $K_{\mu 3}$ background, we used the angular correlation between muon and photon. In the case of the IB, INT_, and SD_ terms of the $K_{\mu\nu\gamma}$ decay, the photon is preferably emitted to the same direction as μ^+, while in the case of $K_{\mu 3}$ decay one of the two photons from the π^0 decay will go to the opposite direction of μ^+.

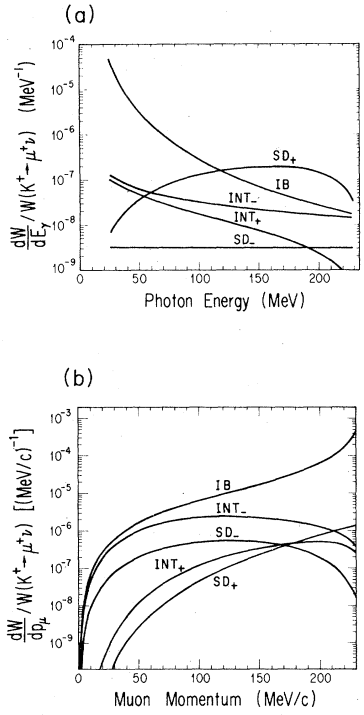

FIG. 3. (a) Differential rates relative to the $K^+\to\mu^+\nu$ total rate $W(K^+\to\mu^+\nu)$ as a function of photon energy. The differential rates were obtained by integrating over the momentum region $215 < p_\mu < 230$ MeV/c. The following values were assumed for the form factors: $|F_V+F_A|M_K = |F_V-F_A|M_K = 0.3$. (b) Differential rates relative to the $K^+\to\mu^+\nu$ total decay rate $W(K^+\to\mu^+\nu)$ as a function of muon momentum. The form factors were taken as same as in (a).

The large solid angle (90% of 4π sr) covered by the photon detector of our apparatus made it possible to reject the $K_{\mu 3}$ mode efficiently based on this difference of μ^+-γ angular correlation.

III. THE EXPERIMENT AND THE DATA TAKING

The experiment was performed at the low-energy separated beam line K3 of the National Laboratory for High Energy Physics (KEK) 12-GeV proton synchrotron. A plan view of the experimental apparatus is shown in Fig. 4. Although the details of the experiment will be published in a separate paper,[5] we briefly describe the essential points of the apparatus.

Positive kaons of 550 MeV/c extracted from the K3 beam line were degraded by a copper degrader and stopped in a target. In the trigger stage, kaons were selected by two sets of Lucite Čerenkov counters. In off-line analyses, kaons were unambiguously identified by the pulse heights of the Čerenkov counters and the time of flight along the beam line. The target consisted of 14 layers of plastic scintillation counters (target counters). The thickness of each layer was 3 (for 12 layers) or 2 mm (for 2 layers). The stopping and decay position of the kaon was determined by the timing and pulse height from the target counters.

The momentum of the charged particle from the K^+ decay was analyzed by a magnetic spectrometer equipped with four sets of bidimensional-readout multiwire proportional chambers (MWPC's), and was determined by the least-squares fitting to the particle track. The pole faces of the spectrometer magnet was covered by veto counters which helped to reject the particles which were scattered on the pole faces. Spurious events such as π^+ decay in flight were eliminated by using the χ^2 value calculated in the fitting procedure.

The momentum determined by the spectrometer was corrected for by using the energy loss measured in the target counters. The dE/dx values measured in the target counter array were also used to reject spurious events such as K^+ decay in flight in the target and nuclear reaction of π^+ in the target.

The momentum resolution of the spectrometer was 1.6 MeV/c (FWHM) at the 235.5-MeV/c μ^+ peak from the $K_{\mu 2}$ decay after the correction of the energy loss in the target. The momentum range covered by the spectrometer was from 110 to 260 MeV/c.

The time of flight (TOF) of the particle between an entrance counter and an array of counters after the MWPC4 was measured to identify particle species (π, μ, or e). The time resolution of the TOF system was 600 psec (FWHM). The range of the charged particle was also measured by a scintillation-counter array placed after the TOF stop counters.

Photons from the K^+ decay were detected by a photon detector system surrounding the target counters. The photon detector consisted of 206 units of NaI(Tl) crystals (6.3 cm$\times$6.3 cm$\times$30 cm). Among them, 88 NaI(Tl) crystals were placed between the target and the spectrometer magnet, and an array of 10$\times$10 crystals was placed opposite to the spectrometer. Others were placed in the

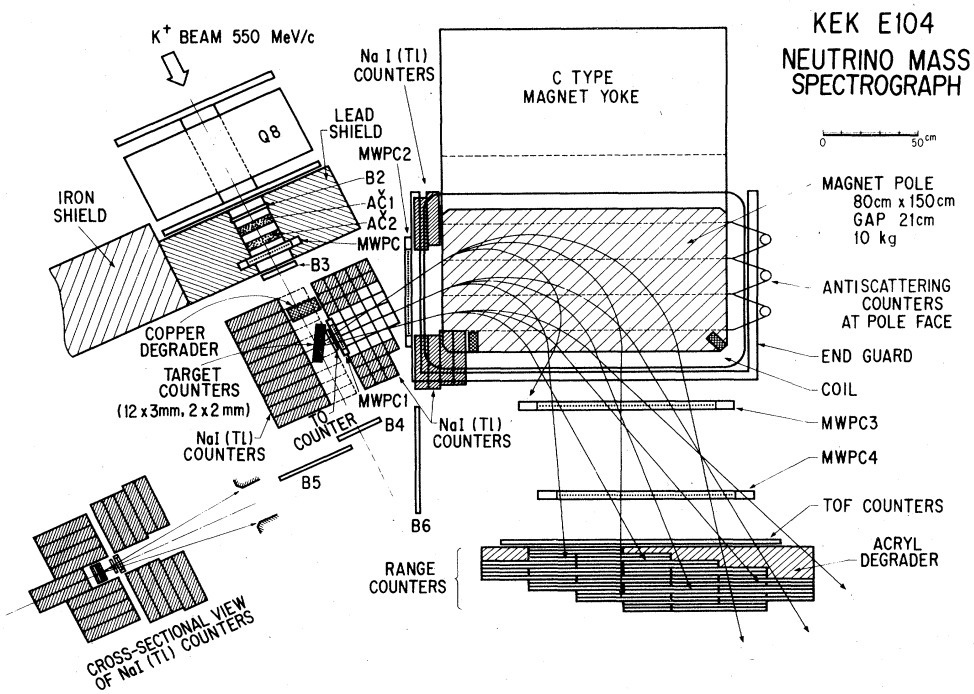

FIG. 4. A plan view of the experimental apparatus.

pole gap of the spectrometer magnet. Each crystal was viewed by a photomultiplier tube. The output signals from the photomultiplier tubes were summed up with their neighbors and 73 independent signals were registered. The solid angle covered by the detector was about 90% of 4π sr.

The timing as well as the pulse height from the photon detector was recorded. The timing was used to reject the accidental hits on the photon detector. The sources of these accidentals were the beam halo and the fast neutrons around the experimental area. The threshold energy for the timing measurement was set below 0.5 MeV.

The photon detector system was designed to have a very wide dynamic range of energy measurement from 0.5 to 300 MeV. In order to cover this wide dynamic range without losing the accuracy of the energy measurement in the low-energy region, we used two analog-to-digital converters (ADC's) for each of the 73 independent signals from the photon detector. The signal was divided into two with the pulse-height ratio of 10:1 and each divided signal was fed into an ADC. The maximum measurable energy of one ADC was adjusted to 30 MeV and that of the other was 300 MeV. The gain of each unit of NaI(Tl) was calibrated within 10% by using γ-ray sources. The gain drift was checked every two weeks and was found to be less than 10%. The energy resolution of the photon detector was about 25% FWHM for the 245 MeV π^0 from the $K_{\pi 2}$ decay, as shown in Fig. 5.

The trigger had the following configuration:

$$\text{trigger} = (K_{\text{stop}}) \cdot (T0) \cdot (\text{TOF}_{\text{stop}}) \cdot (\overline{\text{VETO}}) \,, \tag{8a}$$

$$K_{\text{stop}} = (K^+_{\text{beam}}) \cdot \left[\prod_{i=1}^{14} \text{ST}_i \right] \,, \tag{8b}$$

where ST_i is the ith layer of the stopping counters and $T0$ was the start counter for the TOF measurement. TOF_{stop} is a logical sum of the TOF stop counters and VETO is a logical sum of the veto counters placed on the pole faces of the magnet. K_{beam} was defined by two plastic scintillation counters and two sets of Lucite Cerenkov counters placed along the K3 beam line. This trigger condition only required that the incident particle was a kaon and a charged particle passed through the spectrometer.

The data were handled by an intelligent CAMAC branch driver CCS-11 developed by Hayano and was recorded on magnetic tapes through a PDP-11/34 computer. The trigger rate was about 30 per 2.5-sec beam spill cycle of the KEK proton synchrotron.

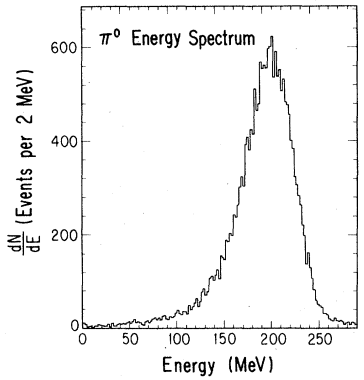

FIG. 5. E_γ spectrum for the $K_{\pi 2}$ events observed by the photon detector. The average observed energy is smaller than the total energy of π^0 (245 MeV) because of the leakage of the shower.

IV. ANALYSIS AND RESULTS

A. Muon momentum spectrum

The momentum spectrum of muons is shown in Fig. 6(a). Muons are identified by the TOF by requiring that the deviation of the measured TOF from the expected TOF for muons is less than 6%.

The peak at 235.5 MeV/c comes from the $K_{\mu 2}$ decay and the smaller peak at 205 MeV/c comes from the $K_{\pi 2}$ decay due to π/μ misidentification. The probability that a pion is misidentified as a muon was about 20% at this momentum. In the momentum region where the $K_{\pi 3}$ decay opens ($p_\pi < 133$ MeV/c) the probability of π/μ misidentification is much smaller (2%).

For the case of μ/e separation, the probability that a positron is misidentified as a muon is 2% for $p_e = 200$ MeV/c and smaller for lower momentum. The continuum below 215 MeV/c mainly comes from the $K_{\mu 3}$ decay. The lower-momentum tail of the $K_{\mu 2}$ peak is due to the $K_{\mu\nu\gamma}$ decay.

A scatter plot of the muon momentum p_μ and the energy deposit in the photon detector E_γ is shown in Fig. 6(b). In this figure, the $K_{\mu 2}$ events are concentrated at $p_\mu = 235.5$ MeV/c and $E_\gamma = 0$ MeV, while the $K_{\pi 2}$ events and the $K_{\mu 3}$ events are characterized by their large E_γ values from the π^0 associated with these decay modes. The events around $p_\mu = 235$ MeV/c with large E_γ values

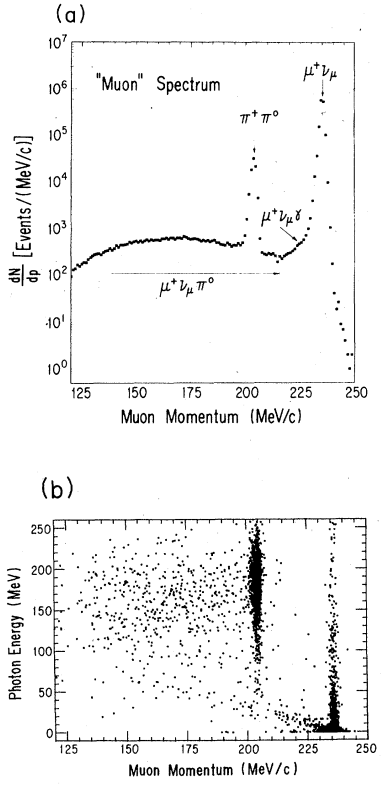

FIG. 6. (a) Observed momentum spectrum of muon. (b) Scatter plot of p_μ and E_γ. The amount of the data presented in (b) is only a small part of the total event analyzed.

are due to the accidental hits in the photon detector. These events mimic the $K_{\mu\nu\gamma}$ events and make a serious background for the observation of the $K_{\mu\nu\gamma}$ mode. The contamination of this background was avoided by selecting the momentum region of $p_\mu < 231.5$ MeV/c in the analysis.

B. Measurement of the IB term

We measured the branching ratio of the IB term from the momentum spectrum of muons between 214.5 and 231.5 MeV/c. A muon momentum spectrum which is gated by the condition $E_\gamma > 1.0$ MeV is shown in Fig. 7. This condition was applied to enrich the $K_{\mu\nu\gamma}$ events and to reject the background from the non-Gaussian tail of the $K_{\mu 2}$ peak. This spectrum corresponds to the total $K_{\mu 2}$ event of 1.40×10^6 before the E_γ cut.

The remaining $K_{\mu 2}$ events at $p = 235.5$ MeV/c mainly come from the accidental hit in the photon detector. We evaluate the probability of the accidental hit as 7.5% from the survival ratio of this $K_{\mu 2}$ peak after the E_γ cut. The correction for the spectrometer acceptance and the photon detection efficiency, and background subtraction were applied to this spectrum in the following way.

The acceptance relative to the 235.5-MeV/c $K_{\mu 2}$ peak was evaluated by a Monte Carlo simulation for each momentum. The result of the Monte Carlo simulation was checked by using the spectrum of the $K_{\mu 3}$ events and the amount of the $K_{\pi 2}$ events measured concurrently in the experiment. The obtained acceptance was a smooth function of p_μ and varied from 1.12 ± 0.02 at $p_\mu = 215$ MeV/c to 1.03 ± 0.01 at $p_\mu = 230$ MeV/c as shown in Fig. 8.

The detection efficiency for photons from the IB component was estimated by a Monte Carlo simulation based on an electromagnetic-shower simulation program EGS.[6] The result showed that the detection efficiency was (85 ± 3)% and almost independent of the muon momentum in the momentum region 214.5–231.5 MeV/c.

There were two major sources of the background. They

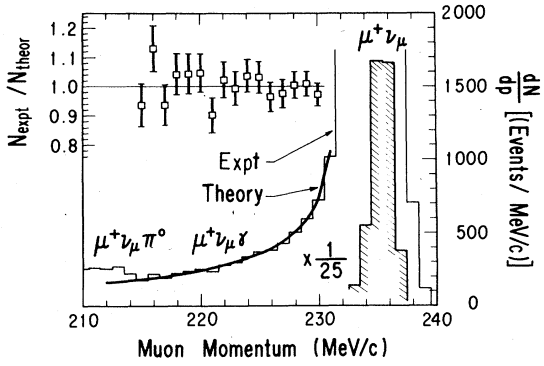

FIG. 7. A momentum spectrum of μ^+ with the condition $E_\gamma > 1.0$ MeV. The peak at $p_\mu = 235$ MeV/c is the $K_{\mu 2}$ peak with accidental hit in photon counters. The solid line represents the p_μ spectrum calculated from the IB term. The inset shows the ratio of the experimental value to the theory as a function of p_μ.

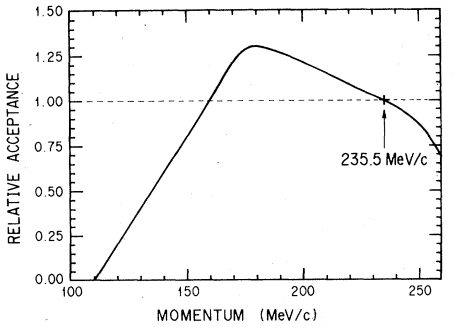

FIG. 8. The acceptance of the spectrometer as a function of the muon momentum. The acceptance for 235.5 MeV/c muons were normalized to 1.

were (i) K_{e3} events with μ/e misidentification, and (ii) the leakage from the tail of the $K_{\mu 2}$ peak due to accidental hits in the photon detector.

The amount of the background coming from (i) was estimated by the positron momentum spectrum multiplied by the μ/e misidentification probability of 2%. The estimated number of the K_{e3} background in each momentum bin was only a few events, and thus was negligible for the present analysis.

In order to evaluate the leakage from the $K_{\mu 2}$ event, we assumed the following relations:

$$N_0 = N_{\mu\nu\gamma} + N_{\mathrm{BG}} , \tag{9a}$$

$$N_\gamma = N_{\mu\nu\gamma} e_\gamma + N_{\mu\nu\gamma}(1-e_\gamma) d_\gamma + N_{BG} d_\gamma , \tag{9b}$$

where

$$N_0 = \text{number of events before the } E_\gamma \text{ cut} , \tag{10a}$$

$$N_{\mu\nu\gamma} = \text{number of true } K^+ \to \mu^+ \nu\gamma \text{ events} , \tag{10b}$$

$$N_{\mathrm{BG}} = \text{number of background events} , \tag{10c}$$

$$N_\gamma = \text{number of events after the } E_\gamma \text{ cut} , \tag{10d}$$

$$e_\gamma = \text{detection efficiency for photons (85\%)} , \tag{10e}$$

$$d_\gamma = \text{probability of the accidental hit on the photon detector (7.5\%)} . \tag{10f}$$

The amount of the estimated background was very small, less than 1% in the momentum region $215 < p_\mu < 230$ MeV/c. In particular, N_{BG} was consistent with 0 within statistical errors in the region $p_\mu < 220$ MeV/c. However, N_{BG} increased as p_μ approached 235.5 MeV/c and the correction was 8% for the 230-MeV/c bin. The background from other decay modes such as $K^+ \to \mu^+ \nu e^+ e^-$ were completely negligible because of their small branching ratios.

Now we compare the observed spectrum with the theoretical one. The theoretical spectrum was calculated by taking only the IB component into account. The acceptance for each momentum bin and the photon detection efficiency were taken into account. The ratio of the experimental value to the calculation for each momentum bin was consistent with 1.0 within errors as shown in the inset of Fig. 7. In this figure, only the statistical errors are quoted.

By integrating over the momentum region $214.5 < p_\mu < 231.5$ MeV/c we obtained the result

$$\text{experiment/theory} = 0.991 \pm 0.013(\text{stat}) / \pm 0.03(\text{syst}) , \tag{11}$$

where the second and third terms represent the statistical error and the systematic error. The overall systematic error, which comes mainly from the uncertainty of the photon detector efficiency, was estimated to be less than 3%.

C. SD_+ term

We searched for the effect of the SD_+ component in a momentum region of $216 < p_\mu < 230$ MeV/c requiring that the energy deposit E_γ should be larger than 100 MeV. By this E_γ cut, more than 99% of the IB component was eliminated. The main sources of the remaining background were (i) the K_{e3} decay with μ/e misidentification, and (ii) the accidental hits in the photon detector. Contrary to the analysis of the IB term, the background from the K_{e3} decay was very serious for the present case because most of the K_{e3} events passed the E_γ cut.

In addition to the E_γ cut we imposed a "pattern cut" which requires following conditions on the pattern of energy deposit in the NaI counter array to reduce these backgrounds. They were as follows: (1) Only one cluster of large energy deposit should be recorded in the central 4×4 array of NaI(Tl) crystals placed in the opposite side of the spectrometer, and (2) there should be no energy deposit in the NaI(Tl) array placed in the spectrometer side. Conditions (1) and (2) ensured the μ^+-γ angular correlation allowed by the kinematics of the SD_+ component and eliminated the background from the IB component with accidental hit in the backward 10×10 NaI(Tl) crystals. Condition (1) eliminated the background from the K_{e3} mode because two photons from the decay of π^0 emitted in this mode would make two clusters.

The survival ratio of the $K_{\mu\nu\gamma}(SD_+)$ events was calculated by a Monte Carlo simulation using the EGS code. It was found that 80% of the SD_+ events with an energy deposit larger than 100 MeV in the central 4×4 NaI(Tl) crystals (this condition is added later) pass the "pattern cut."

As a check of the Monte Carlo program, we compared the E_γ spectrum expected from the simulation with the observed one. The observed E_γ spectrum in the central 4×4 NaI(Tl) crystals for those events which passed the "pattern cut" is shown in Fig. 9(a), together with the expected spectrum calculated by the Monte Carlo simulation taking account of only the IB component. In this calculation, the number of the Monte Carlo events was normalized to the total number of $K_{\mu 2}$ peak events (1.4×10^6). From this comparison, we concluded that the error of the correction factor which was introduced by the pattern cut was less than 10%.

In addition to the pattern cut we selected the events with energy deposit greater than 100 MeV in the central 4×4 NaI(Tl) crystals. The survival ratios after the pat-

tern cut and this selection were estimated to be $(40\pm10)\%$ for the IB component and $(62\pm10)\%$ for the SD_+ component. The quoted error corresponds to the change of the E_γ threshold (100 MeV) by ±20 MeV.

The momentum spectrum of those events which passed all these event selections is shown in Fig. 9(b). The structure below 215 MeV/c comes from the $K_{\mu3}$ decay. The surviving $K_{\mu2}$ peak contained 35 events out of 1.4×10^6 events. Therefore, the rate of the accidental coincidence to the condition $E_\gamma > 100$ MeV was 4×10^{-5}.

There were eight events in the momentum region $216 < p_\mu < 230$ MeV/c and these events were $K_{\mu\nu\gamma}$ candidates. The number of events in this region expected from the IB component was calculated as 6 ± 2 by the Monte Carlo simulation.

The background from the K_{e3} decay was estimated from the number of positron events passing the same event selection and found to be less than 0.5 events. The background from the $K_{\mu2}$ with accidental coincidence was estimated from the number of events surviving at the $K_{\mu2}$ peak. It was about 0.1 events. Therefore, 2 ± 3.44 events (the error is one standard deviation) were attributed to the SD_+ term.

Theoretically, the expected number of the SD_+ events is expressed as

$$N(\mathrm{SD}_+,\mathrm{theory}) = N(K_{\mu\nu}) \int_{216\ \mathrm{MeV}/c}^{230\ \mathrm{MeV}/c} \frac{dW(\mathrm{SD}_+, E_\gamma > 100\ \mathrm{MeV})}{dp} dp\,(0.62\pm0.10)\times[(F_V+F_A)M_K]^2$$

$$= (1.4\times10^6)\times(1.83\times10^{-4})\times(0.62\pm0.10)\times[(F_V+F_A)M_K]^2\,, \tag{12}$$

where $N(K_{\mu\nu})=1.4\times10^6$ is the total number of $K_{\mu\nu}$ events.

Thus by comparing formula (12) and 2 ± 3.44, the upper bound for $|F_V+F_A|M_K$ is calculated as

$$|F_V+F_A|M_K < 0.23 \quad (90\%\ \mathrm{C.L.})\,. \tag{13}$$

In this calculation $[(F_V+F_A)M_K]^2$ was taken as positive number (both F_V and F_A were assumed to be real). This bound indicates that the contribution of (SD_+ term + INT_+ term) to the total branching ratio of $K_{\mu\nu\gamma}$ is less than 1%.

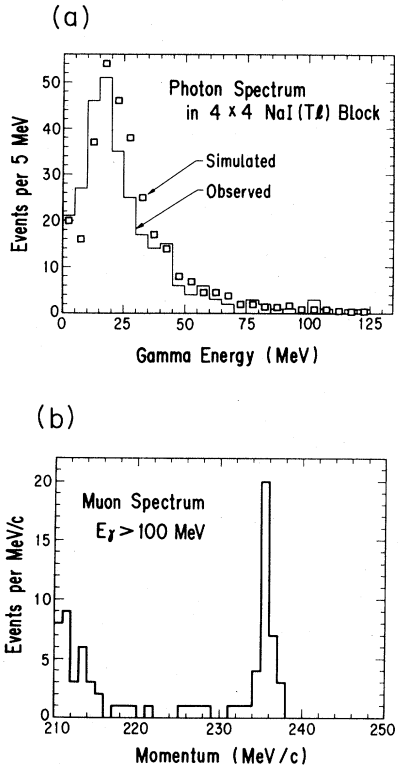

FIG. 9. (a) Photon energy spectrum observed in the central 4×4 NaI(Tl) crystals (histogram), and simulated one (squares). The condition of the event selection for the measured spectrum is described in the text. (b) Observed momentum spectrum of muon with energy deposit greater than 100 MeV in the central 4×4 NaI(Tl) crystals.

D. SD_- and INT_- term

We searched for the effect of the SD_- term and the INT_- term in the kinematical region $120 < p_\mu < 150$ MeV/c. As mentioned in Sec. II, the background from the $K_{\mu3}$ decay was very serious. We imposed the following conditions to reject the background from the $K_{\mu3}$ mode: (1) The energy deposit in the 10×10 NaI(Tl) array in the opposite side of the spectrometer should be less than 1 MeV, and (2) the sum of the energy deposits in the NaI(Tl) counters located in the spectrometer side should be greater than 1 MeV. These conditions required that the photon should be emitted in the same direction as μ^+, and thus rejected most of the $K_{\mu3}$ events because one of the decay photons from π^0 would go to the backward direction of μ^+.

Figure 10 shows a scatter plot of p_μ and E_γ for the events passing this event selection. By comparing this figure with Fig. 6(b), we find that the $K_{\pi2}$ events and most of the $K_{\mu3}$ events are eliminated by this cut and only $K_{\mu\nu\gamma}$-like events remain.

The veto efficiency for the $K_{\mu3}$ events was estimated to be greater than 99% by a Monte Carlo simulation. As a check of this estimation for the veto efficiency, we applied the same event selection to the K_{e3} events. Since the kinematics of the K_{e3} is almost the same as that of the $K_{\mu3}$, the veto efficiency for the former is very similar to that of the latter. We compared the calculated veto efficiency for the K_{e3} event to the experimental value. Then we found that the two values agreed within the statistical error of 15%. Therefore, we estimated the error of the Monte Carlo result for the $K_{\mu3}$ mode was less than 15%.

Conditions (1) and (2) were also very effective to reduce

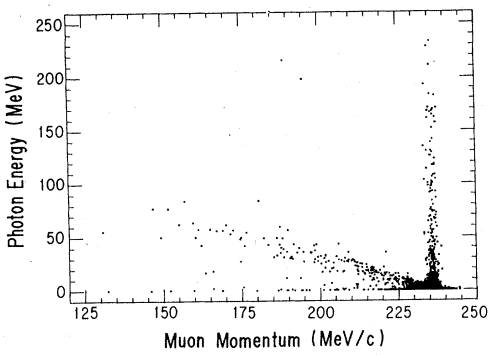

FIG. 10. A scatter plot of p_μ and E_γ of the events without energy deposit in the backward NaI(Tl) crystals. The amount of the data presented in this figure is only a fraction of total data analyzed.

the background from the $K_{\pi 3}$ decay modes. These modes were strongly suppressed by condition (1) because one of their decay products would hit the NaI(Tl)'s placed opposite to the spectrometer. In order to evaluate the number of background events from these modes, we applied the same event selection to the π^+ spectrum. The number of π^+ events passing the cut was only 12. Considering the small probability of μ/π misidentification (about 2% in this momentum range), we safely neglected these backgrounds. The backgrounds from other decay modes such as $K^+ \to \mu^+ \nu\pi^+\pi^-$ were also negligible because of their small branching ratios.

We estimated the fraction λ of the accepted events with conditions (1) and (2) for each component of the $K_{\mu\nu\gamma}$ decay by a Monte Carlo simulation. The results were $\lambda(\mathrm{IB})=40\%$, $\lambda(\mathrm{INT\_})=25\%$, and $\lambda(\mathrm{SD\_})=15\%$ and were almost constant in the momentum region $120<p_\mu<150$ MeV/c. The different values of λ came from the difference of the μ^+-γ angular correlation between these three components.

The reliability of this Monte Carlo simulation was checked by applying the same conditions to the experimental data in the momentum region of $210<p_\mu<230$ MeV/c where the contribution of the IB term is dominant. The ratio $(55\pm1)\%$ of the accepted events for the experimental data agreed with the ratio $(56.6\pm1)\%$ estimated by the Monte Carlo simulation.

Now, let us search for the effect of the INT_ term and the SD_ term by comparing the number of the accepted events in the momentum region $120<p_\mu<150$ MeV/c with the theoretical calculation. Since we can neglect the contributions of the INT_+ term and the SD_+ term, we obtain the following expression for the expected number of the $K_{\mu\nu\gamma}$ events by integrating Eq. (3) over the kinematical region corresponding to $120<p_\mu<150$ MeV/c:

$$N(\text{theory}) = N(K_{\mu\nu})\lambda(\mathrm{IB})\times 2.00\times 10^{-4} + N(K_{\mu\nu})\lambda(\mathrm{INT\_})\times 1.17\times 10^{-4}\times(F_V-F_A)M_K + N(K_{\mu\nu})\lambda(\mathrm{SD\_})\times 0.89\times 10^{-4}\times[(F_A-F_A)M_K]^2 , \quad (14)$$

where $N(K_{\mu\nu})=1.9\times 10^6$ is the total number of observed $K_{\mu\nu}$ events. The momentum dependence of the spectrometer acceptance and the efficiency of the E_γ conditions (1) and (2) are taken into account in this integration.

The expected number for the first term was calculated as 152, while the observed number of events which passed the event selection was 178. On the other hand, the number of $K_{\mu 3}$ background among the observed events was estimated as 36 ± 8. Therefore 142 events were $K_{\mu\nu\gamma}$ candidates. Thus we get a quadratic equation

$$25.3[(F_V-F_A)M_K]^2 + 55.4(F_V-F_A)M_K = -10\pm 18 , \quad (15)$$

where the quoted error (one standard deviation) includes the statistical error for the observed number 178 and the systematic error for the estimated number 152 due to the uncertainty in the acceptance correction. By solving Eq. (15) we obtained a bound for the value of F_V-F_A as

$$-2.5 < (F_V-F_A)M_K < 0.3 \quad (90\%\ \text{C.L.}) . \quad (16)$$

This result and the corresponding result obtained from a study of the $K^+ \to e^+\nu\gamma$ mode[2] are shown in Fig. 11. The lower bound on F_V-F_A was rather loose because the contributions from the SD_ term and the INT_ term cancel each other in the negative region of F_V-F_A. The contribution of (SD_ term + INT_ term) to the total decay rate of K^+ is also shown in Fig. 11.

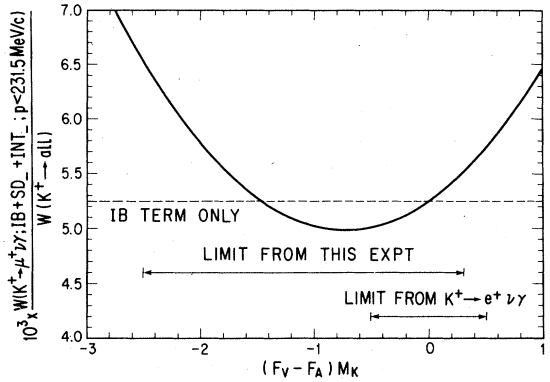

FIG. 11. Partial decay rate of (IB term + SD_ term + INT_ term) in the momentum region $p_\mu<231.5$ MeV/c normalized by the $K^+ \to \mu^+\nu$ total decay rate $W(K^+\to\mu^+\nu)$ as a function of $(F_V-F_A)M_K$. The limit on $(F_V-F_A)M_K$ obtained from this experiment is presented with the limit from the $K_{e\nu\gamma}$ experiment of Ref. 2.

V. CONCLUSION

Now we summarize the results of this experiment.

(i) The muon momentum spectrum from $K_{\mu\nu\gamma}$ decay was measured in the range of $214.5 < p_\mu < 231.5$ MeV/c. the obtained spectrum was in good agreement with the QED calculation assuming only the IB term. The ratio of the experimental decay rate to the theoretical one was found as

$$\text{experiment/theory} = 0.991 \pm 0.013(\text{stat}) \pm 0.03(\text{syst}) .$$

In other words, the branching ratio was found to be

$$\frac{W(K \to \mu\nu\gamma, 214.5 < p_\mu < 231.5 \text{ MeV}/c)}{W(K \to \text{all})} = (3.02 \pm 0.10) \times 10^{-3} \quad (17)$$

or

$$\frac{W(K \to \mu\nu\gamma, p_\mu < 231.5 \text{ MeV}/c, \text{IB term})}{W(K \to \text{all})} = (5.42 \pm 0.18) \times 10^{-3} . \quad (18)$$

(ii) Bounds on the form factors of vector and axial-vector currents are obtained as

$$|F_V + F_A| M_K < 0.23 , \quad (19a)$$

$$-2.5 < (F_V - F_A) M_K < 0.3 , \quad (19b)$$

or, in terms of the branching ratio,

$$\frac{W(K \to \mu\nu\gamma, \text{SD}_+)}{W(K \to \text{all})} < 3.0 \times 10^{-5} , \quad (20a)$$

$$\left| \frac{W(K \to \mu\nu\gamma, \text{INT}_+)}{W(K \to \text{all})} \right| < 2.7 \times 10^{-5} , \quad (20b)$$

$$\left| \frac{W(K \to \mu\nu\gamma, \text{SD}_- + \text{INT}_-)}{W(K \to \text{all})} \right| < 1.3 \times 10^{-3} . \quad (20c)$$

If we assume the μ-e universality and also neglect the q^2 dependence of the form factors, the obtained values of the form factors can be directly compared with the form factors of the $K_{e\nu\gamma}$ mode. Our result is consistent with the value of the $K_{e\nu\gamma}$ form factors [Eqs. (1a) and (1b)]. If we combine our result with the constraints obtained by the $K_{e\nu\gamma}$ experiment, the large negative value of $F_V - F_A$ is excluded. In this case, the contribution from the $\text{INT}_- + \text{SD}_-$ is evaluated as (see Fig. 11)

$$\left| \frac{W(K \to \mu\nu\gamma, \text{SD}_- + \text{INT}_-)}{W(K \to \text{all})} \right| < 2.6 \times 10^{-4} , \quad (21)$$

or the branching ratio of the $K_{\mu\nu\gamma}$ mode including the structure dependent terms is

$$\frac{W(K \to \mu\nu\gamma, p_\mu < 231.5 \text{ MeV}/c)}{W(K \to \text{all})} = (5.4 \pm 0.3) \times 10^{-3} . \quad (22)$$

ACKNOWLEDGMENTS

We would like to acknowledge Professor T. Nishikawa, Professor S. Ozaki, Professor A. Kusumegi, Professor H. Sugawara, and Professor H. Hirabayashi for encouragement and support of the present experiment at KEK. We thank Dr. S. R. Schnetzer for his contribution in the early stage of this study. We thank the crew of the accelerator, beam channel, and experimental facilities of the KEK PS for their excellent operation. This work is partially supported by the Grant-in-Aid for Co-operative Research of the Japanese Ministry of Education, Science and Culture.

[1] D. E. Neville, Phys. Rev. **124**, 2037 (1961); A. Q. Sarker, *ibid.* **173**, 1749 (1968); H. Namaizawa, Prog. Theor. Phys. **39**, 860 (1968); R. Rockmore, Phys. Rev. **177**, 2573 (1969); N. J. Carron and R. L. Schult, Phys. Rev. D **1**, 3171 (1970); M. G. Smoes, Nucl. Phys. **B20**, 237 (1970); D. Y. Bardin and S. M. Bilen'kii, Yad. Fiz. **16**, 557 (1972) [Sov. J. Nucl. Phys. **16**, 311 (1973)]; K. A. Milton and W. W. Wada, Phys. Lett. **98B**, 367 (1981). There is an excellent review article for the related process $\pi \to e\nu\gamma$; D. A. Bryman, P. Depommier, and C. Leroy, Phys. Rep. **88**, 151 (1982). Many useful references are found therein. For the definition of the form factors, we followed the notation of S. G. Brown and S. A. Bludman, Phys. Rev. **136**, 1160 (1964); J. N. Huang and C. Y. Lee, Phys. Rev. D **27**, 2227 (1983).

[2] J. Heintze *et al.*, Nucl. Phys. **B149**, 365 (1979).

[3] A. O. Weissenberg *et al.*, Phys. Lett. **48B**, 474 (1974).

[4] The first result of these searches was published in R. S. Hayano *et al.*, Phys. Rev. Lett. **49**, 1305 (1982), and T. Yamazaki *et al.*, *ibid.* **52**, 1089 (1984). The results of the second experiment which was performed concurrently with the present work is to be published.

[5] T. Yamazaki *et al.* (unpublished).

[6] R. L. Ford and W. R. Nelson, Report Nos. SLAC-210 and UC-32, 1978 (unpublished).